Transient waves from internal sources in non-stationary media - Numerical implementation

Åberg, Ingegerd

1996

CODEN:LUTEDX/(TEAT-7048)/1-29/(1996)

Transient waves from internal sources in non-stationary media — Numerical implementation

Ingegerd Åberg

Department of Electroscience
Electromagnetic Theory
Lund Institute of Technology
Sweden

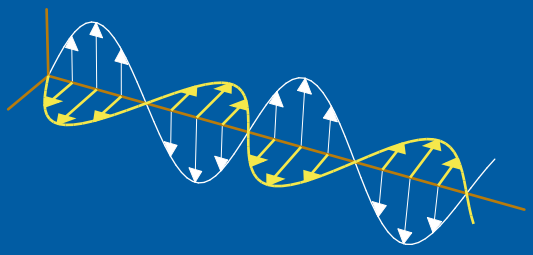

Ingegerd Åberg

Department of Electromagnetic Theory
Lund Institute of Technology
P.O. Box 118
SE-221 00 Lund
Sweden

Editor: Gerhard Kristensson

Abstract

In this paper, the focus is on numerical results from calculations of scattered direct waves, originating from internal sources in non-stationary, dispersive, stratified media. The mathematical starting point is a general, inhomogeneous, linear, first order, 2×2 system of equations. Particular solutions are obtained, as integrals of waves from point sources distributed inside the scattering medium. Resolvent kernels are used to construct time dependent fundamental wave functions at the location of the point source. Wave propagators, closely related to the Green functions, at all times advance these waves into the surrounding medium. Two illustrative examples are given. First waves, propagating from internal sources in a Klein-Gordon slab, are calculated with the new method. These wave solutions are compared to alternative solutions, which can be obtained from analytical fundamental waves, solving the Klein-Gordon equation in an infinite medium. It is shown, how the Klein-Gordon wave splitting, which transforms the Klein-Gordon equation into a set of uncoupled first order equations, can be used to adapt the infinite Klein-Gordon solutions to the boundary conditions of the Klein-Gordon slab. The second example hints at the extensive possibilities offered by the new method. The current and voltage waves, evoked on the power line after an imagined strike of lightning, are studied. The non-stationary properties are modeled by the shunt conductance, which grows exponentially in time, together with dispersion in the shunt capacitance.

1 Background

In the early 1980s, in an attempt to facilitate the study of wave propagation problems in the time domain, some papers appeared combining the concepts of wave-splitting and invariant imbedding [9, 10, 13]. Both of these tools had been known a priori. The origin of the wave-splitting is not known for sure, but it certainly had been used by frequency domain mathematicians for some time [6, 8]. The invariant imbedding had its start from around 1940, and then developed gradually [4, 7]. The new ideas proved effective and much effort has since been put in to further refine them. One useful idea, which opened new possibilities, was the one giving rise to the Green functions technique [19]. A broad variety of problems have been analyzed with these methods. Many different types of media have been investigated. First transient electro-magnetic wave propagation in dissipative media was studied [17], and around the same time there was an extension to dispersive media [5]. Later on, more complex media have been thoroughly examined, e.g. bi-isotropic media [18], gyrotropic media [22], and anisotropic media [14]. The most common approach is to let the scattering medium be confined to a slab, which is then exposed to impinging electro-magnetic waves. There are two ways to formulate the leading question: In the direct scattering problem, the scattering medium is known, and the search is for the reflected and transmitted waves. In the inverse problem, on the other hand, the scattering medium is unknown, so the aim is to infer information about its hidden properties. This can be done, if sufficient information about the scattered waves

is extracted by experimental measurements. Other geometries, than the slab, have been investigated, e.g. the cylinder [15] and the waveguide [16, 21]. A challenge of great interest today, is to solve transient wave propagation problems in three dimensions. Some interesting results have been reported [25, 26].

In all studies mentioned so far, the presumption is that the properties of the scattering medium are invariant in time. This means that the coefficients of the wave equation only depend on spatial coordinates. In some recent investigations [1–3], this presumption is abandoned, and the analysis has been extended to treat transient wave propagation problems in non-stationary media. Again, the scattering medium is confined to a slab. However, the properties of the medium change quickly in time. The wave equations have coefficients depending on one spatial coordinate and time. The relevant time scale of the variation is related to the time it takes the wave to propagate through the non-stationary scatterer.

Many interesting areas of application have been mentioned, e.g. fading and modulation problems within telecommunications, wave propagation on transmission lines, maybe in connection with lightning, pressure waves in the ground at the time of an earthquake, and some problems within electro-mechanical engineering, among them the use of piezo-electric sensors to control continua [24]. Another field calling for attention is the possibility to solve nonlinear problems with the methods developed for non-stationary media. When quasi-linear wave equations are linearized, the resulting equations have coefficients which depend on both time and space.

The first analysis of wave propagation in non-stationary media, with special attention put on the inverse problem, had one main restriction: the wave phase velocity was presumed invariant to time translations [2]. A generalization of the analysis, allowing a time-dependent velocity, was presented in a subsequent paper [3]. In these first two papers the basic wave equations are homogeneous. This means that the sources generating the waves, are external to the scattering medium. A recent investigation, with emphasis on the direct problem, treats waves originating from distributed sources inside the scattering medium [1].

The particular solution of the inhomogeneous wave equation is presented. The work was inspired by Ref. 11, which treats the source problem from the inverse scattering point of view. For uniqueness reasons then, some restrictions have to be put on the form of the source function. By only regarding the direct scattering problem, these restrictions can be avoided. This is necessary, if the analysis is intended to be a step in the development of methods aiming at solving nonlinear wave equations. In this paper, numerical calculations performed on basis of the mathematical theory in Ref. 1 are presented. After a survey of the theory and the algorithms, some guidelines in the realization of the computer-code are discussed in Section 3. Two illustrative examples follow. For a specific medium, an alternative method to obtain the solution has been worked out, and the results of the two calculations are compared. A couple of other examples hint on the further possibilities offered by the new method.

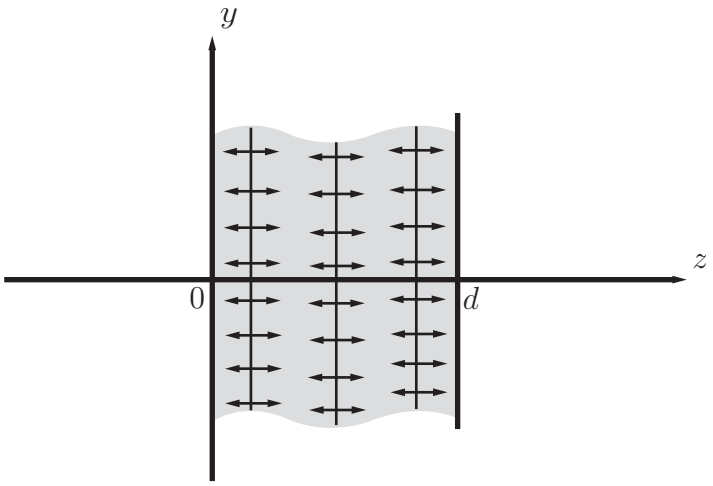

Figure 1: Physical background.

2 Summary of the underlying theory

In this section, parts of the analysis in Ref. 1 is recapitulated. The intention is to provide so much information that the governing ideas can be grasped.

The physical background of the scattering problems considered in this investigation is illustrated in Figure 1. The scattering medium, which is inhomogeneous and non-stationary, is confined to a slab with thickness d. The slab is surrounded by a lossless, homogeneous and time-invariant medium. Inside the slab, there are planar, distributed sources, which transmit both left- and right-going waves. The direction of propagation of all waves in this study is perpendicular to the slab.

The mathematical starting point is a generalized, inhomogeneous set of first order wave equations

$$\begin{aligned}\frac{\partial}{\partial z}\begin{pmatrix}u^+(z,t)\\ u^-(z,t)\end{pmatrix} - f(z,t)\begin{pmatrix}-1 & 0\\ 0 & 1\end{pmatrix}\frac{\partial}{\partial t}\begin{pmatrix}u^+(z,t)\\ u^-(z,t)\end{pmatrix} - \begin{pmatrix}\alpha(z,t) & \beta(z,t)\\ \gamma(z,t) & \delta(z,t)\end{pmatrix}\begin{pmatrix}u^+(z,t)\\ u^-(z,t)\end{pmatrix}\\ - \int_{-\infty}^{t}\begin{pmatrix}A(z,t,t') & B(z,t,t')\\ C(z,t,t') & D(z,t,t')\end{pmatrix}\begin{pmatrix}u^+(z,t')\\ u^-(z,t')\end{pmatrix}dt' = \begin{pmatrix}k^+(z,t)\\ k^-(z,t)\end{pmatrix}\end{aligned} \tag{2.1}$$

The original, dependent wave variables are transformed into the two wave components $u^{\pm}(z,t)$. How this can be done, is demonstrated in some examples in Ref. 3. Here, the concept of wave splitting plays a significant part. Some information about the coefficient functions of (2.1) can be found in Figure 2.

The slowness function f is a positive, continuous, bounded function of the variables z and t everywhere. It is assumed to be constant outside the slab and continuously differentiable, with bounded derivatives, in z and t everywhere inside the slab. The functions α, β, γ and δ are equal to zero outside the slab, and they are continuous, bounded functions inside the slab (not necessarily continuous at the edges of the slab).

The functions A, B, C and D are always zero outside of the slab $(0, d)$. Observe,

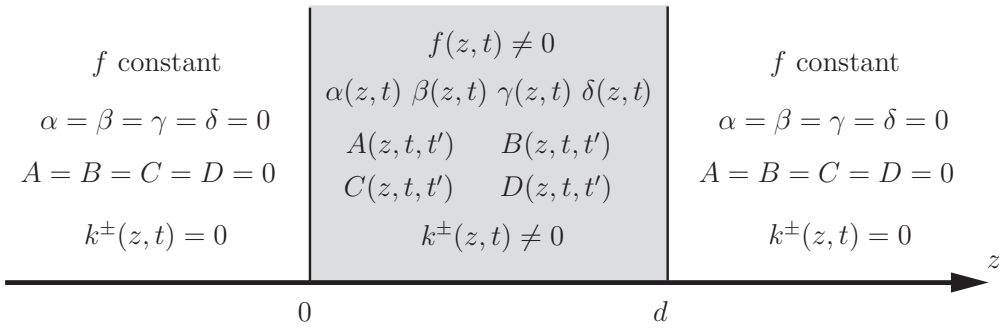

Figure 2: Geometry of the problem.

the double time dependence. The variable t describes the current time, whereas the variable t' is related to the starting time of the excitation. Due to causality, these functions vanish identically inside the slab provided $t < t'$. For simplicity, the functions A, B, C and D are assumed continuous and bounded as functions of the variables z, t and t' in the region $t > t'$, $0 < z < d$.

The source functions $k^{\pm}(z,t)$ are integrable functions in the domain $(z,t) \in (0,d) \times (-\infty, \infty)$. Outside the slab, they vanish identically.

In this part of the analysis, the relevant boundary conditions are

$$\begin{cases} u^{+}(0,t) = 0 \\ u^{-}(d,t) = 0 \end{cases}$$

This means that there are no external sources. Therefore, only the particular solutions of (2.1) are of interest. They model the waves, generated by the internal sources.

In Ref. 1, the solutions of (2.1) are derived in two similar steps. Only one of them is repeated here. The emphasis is then put on waves generated by the source function $k^{+}(z,t)$, so $k^{-}(z,t) = 0$. The solutions of (2.1) are given by

$$\begin{cases} {u_1}^{+}(z,t) = \displaystyle\int_0^z \left\{ \int_{-\infty}^{\tau^{+}(z_0;z,t)} E_{1r}^{+}(z,t;z_0,t_0) k^{+}(z_0,t_0)\, dt_0 \right\} dz_0 \\ \qquad\qquad + \displaystyle\int_z^d \left\{ \int_{-\infty}^{\tau^{-}(z_0;z,t)} E_{1l}^{+}(z,t;z_0,t_0) k^{+}(z_0,t_0)\, dt_0 \right\} dz_0 \\ {u_1}^{-}(z,t) = \displaystyle\int_0^z \left\{ \int_{-\infty}^{\tau^{+}(z_0;z,t)} E_{1r}^{-}(z,t;z_0,t_0) k^{+}(z_0,t_0)\, dt_0 \right\} dz_0 \\ \qquad\qquad + \displaystyle\int_z^d \left\{ \int_{-\infty}^{\tau^{-}(z_0;z,t)} E_{1l}^{-}(z,t;z_0,t_0) k^{+}(z_0,t_0)\, dt_0 \right\} dz_0 \end{cases} \tag{2.2}$$

Here ${E_1}^{\pm}$ are the solutions of the fundamental set of equations, which is obtained if the right side matrix

$$\begin{pmatrix} k^{+}(z,t) \\ k^{-}(z,t) \end{pmatrix}$$

is replaced by the point source matrix

$$\begin{pmatrix} \delta(z-z_0)\delta(t-t_0) \\ 0 \end{pmatrix} \tag{2.3}$$

The subscript r denotes waves observed to the right of the source point $z = z_0$. These waves have wave fronts proceeding along the characteristic traces $t = \tau^+(z; z_0, t_0)$. Vice versa, waves with subscript l are observed in the region $z < z_0$. Their wave fronts travel along the characteristic curves $t = \tau^-(z; z_0, t_0)$.

In the second step, waves generated by the source function $k^-(z,t)$ are calculated, so $k^+(z,t) = 0$. This means that in the source point matrix (2.3), the two elements are interchanged. The solutions ${u_2}^{\pm}(z,t)$ are obtained from (2.2) if subscript 1 is replaced by 2 and k^+ is replaced by k^-. Finally, the solutions of the complete system (2.1) with both source functions $k^{\pm}(z,t) \neq 0$ are obtained after superimposing the two sets of solutions ${u_1}^{\pm}(z,t)$ and ${u_2}^{\pm}(z,t)$, respectively.

The fundamental solutions ${E_1}^{\pm}(z,t;z_0,t_0)$ can be understood as the waves generated in the slab by a right-going impulse introduced at the space-time point (z_0,t_0). Again, the derivation includes two steps. First, the responses ${E_1}^{\pm}(z_0 \pm 0, t; z_0, t_0)$ are calculated. Observe that only waves at the points $z = z_0 \pm 0$ are of interest in this part of the calculation. Since, with exception of the initial δ-pulse, all waves at $z = z_0$ have their origin in the reaction of the medium to the impulse, these waves can be represented by regular functions ${H_1}^{\pm}(z_0, t, t_0)$. Then, in a second step, the fundamental wave expression ${E_1}^{+}(z_0+0, t; z_0, t_0)$ can be propagated to the right into the region $z > z_0$ using propagator expressions derived from Duhamel's integral [12]. For waves propagated to the right, i.e. $z > z_0$, they are

$$\begin{cases} E^+(z,t;z_0,t_0) = p^+(z_0,z,\tau^+(z_0;z,t))E^+(z_0,\tau^+(z_0;z,t);z_0,t_0) \\ \qquad + \displaystyle\int_{-\infty}^{\tau^+(z_0;z,t)} G^+(z_0,z,\tau^+(z_0;z,t),t')p^+(z_0,z,t')E^+(z_0,t';z_0,t_0)\,dt' \\ E^-(z,t;z_0,t_0) = \\ \qquad \displaystyle\int_{-\infty}^{\tau^+(z_0;z,t)} G^-(z_0,z,\tau^+(z_0;z,t),t')p^+(z_0,z,t')E^+(z_0,t';z_0,t_0)\,dt' \end{cases} \tag{2.4}$$

with the wave front factor defined as

$$p^+(z_0,z,t) = \exp\left\{\int_{z_0}^{z} \alpha(\zeta,\tau^+(\zeta;z_0,t))\,d\zeta\right\}$$

The propagation of the fundamental wave expressions ${E_1}^{-}(z_0 - 0, t; z_0, t_0)$ to the left into $z < z_0$ can be described by similar expressions with propagator kernels denoted $Q^{\pm}$. The wave front factor is p^-. The propagator kernels $G^{\pm}$ and $Q^{\pm}$ can be calculated from two initial-boundary value problems of sets of coupled integro-differential first order equations, see Ref. 1.

The final expressions of the propagated fundamental solutions ${E_1}^{\pm}(z,t;z_0,t_0)$

are for $t \geq \tau^+(z;z_0,t_0)$ and $z_0 \leq z \leq d$

$$\begin{cases} {E_{1r}}^+(z,t;z_0,t_0) = p^+(z_0,z,\tau^+(z_0;z,t))\,\delta(\tau^+(z_0;z,t)-t_0) \\ \qquad + p^+(z_0,z,\tau^+(z_0;z,t)){H_1}^+(z_0,\tau^+(z_0;z,t),t_0) \\ \qquad + p^+(z_0,z,t_0)G^+(z_0,z,\tau^+(z_0;z,t),t_0) \\ \qquad + \displaystyle\int_{t_0}^{\tau^+(z_0;z,t)} G^+(z_0,z,\tau^+(z_0;z,t),t')p^+(z_0,z,t'){H_1}^+(z_0,t',t_0)\,dt' \\ {E_{1r}}^-(z,t;z_0,t_0) = p^+(z_0,z,t_0)G^-(z_0,z,\tau^+(z_0;z,t),t_0) \\ \qquad + \displaystyle\int_{t_0}^{\tau^+(z_0;z,t)} G^-(z_0,z,\tau^+(z_0;z,t),t')p^+(z_0,z,t'){H_1}^+(z_0,t',t_0)\,dt' \end{cases} \tag{2.5}$$

and for $t \geq \tau^-(z;z_0,t_0)$ and $0 \leq z < z_0$

$$\begin{cases} {E_{1l}}^-(z,t;z_0,t_0) = p^-(z_0,z,\tau^-(z_0;z,t)){H_1}^-(z_0,\tau^-(z_0;z,t),t_0) \\ \qquad + \displaystyle\int_{t_0}^{\tau^-(z_0;z,t)} Q^-(z_0,z,\tau^-(z_0;z,t),t')p^-(z_0,z,t'){H_1}^-(z_0,t',t_0)\,dt' \\ {E_{1l}}^+(z,t;z_0,t_0) = \\ \qquad \displaystyle\int_{t_0}^{\tau^-(z_0;z,t)} Q^+(z_0,z,\tau^-(z_0;z,t),t')p^-(z_0,z,t'){H_1}^-(z_0,t',t_0)\,dt' \end{cases} \tag{2.6}$$

Due to causality, ${E_{1r}}^\pm(z,t;z_0,t_0) = 0$, $t < \tau^+(z;z_0,t_0)$, and ${E_{1l}}^\pm(z,t;z_0,t_0) = 0$, $t < \tau^-(z;z_0,t_0)$.

A few words should be inserted about the derivation of the expressions for ${H_1}^\pm(z_0,t,t_0)$. They can be obtained, if the fundamental system of equations obtained from (2.1), with the $k^\pm$- function matrix replaced by the δ-function matrix (2.3), is integrated from $z = z_0 - 0$ to $z = z_0 + 0$. This yields two equations in the variable t. These equations can be combined with two other equations, which result if the propagator expressions for G^- and Q^+ are evaluated at $z = z_0 \pm 0$, respectively. The resulting system of equations is

$$\begin{cases} {E_1}^+(z_0+0,t;z_0,t_0) - {E_1}^+(z_0-0,t;z_0,t_0) = \delta(t-t_0) \\ {E_1}^-(z_0+0,t;z_0,t_0) - {E_1}^-(z_0-0,t;z_0,t_0) = 0 \\ {E_1}^-(z_0+0,t;z_0,t_0) = \displaystyle\int_{t_0}^{t} G^-(z_0,z_0,t,t'){E_1}^+(z_0+0,t';z_0,t_0)\,dt' \\ {E_1}^+(z_0-0,t;z_0,t_0) = \displaystyle\int_{t_0}^{t} Q^+(z_0,z_0,t,t'){E_1}^-(z_0-0,t';z_0,t_0)\,dt' \end{cases}$$

From these equations ${E_1}^\pm(z_0 \mp 0,t;z_0,t_0)$ can be eliminated, and the remaining two equations can be solved. One of them is a Volterra equation of the second kind. The unique solution can be constructed using the concept of resolvent kernels. The known function $g(t)$, square integrable in $t \in [t_0,T]$, is related to a function $f(t)$, $t \in [t_0,T]$, by a Volterra equation of the second kind

$$g(t) = f(t) + \int_{t_0}^{t} K(t,t')f(t')\,dt'$$

The kernel $K(t,t')$ is assumed to be square integrable in $(t,t') \in [t_0,T] \times [t_0,T]$. By causality $K(t,t') = 0$, $t < t'$, which explains the upper limit of the integral. This Volterra equation has a unique solution [23] given by

$$f(t) = g(t) + \int_{t_0}^{t} P(t,t')g(t')\,dt'$$

The resolvent kernel $P(t,t')$, which is square integrable in $(t,t') \in [t_0,T] \times [t_0,T]$, is uniquely related to $K(t,t')$. It can be constructed from the integral equation

$$P(t,t') + K(t,t') + \int_{t'}^{t} K(t,t'')P(t'',t')\,dt'' = 0 \tag{2.7}$$

The analysis of Ref. 1 shows that ${H_1}^+(z_0,t,t_0)$ is the resolvent kernel, which can be constructed from equation (2.7) with

$$K(z,t,t_0) = -\int_{t_0}^{t} Q^+(z_0,z_0,t,t')G^-(z_0,z_0,t',t_0)\,dt'$$

and ${H_1}^-$ can be obtained from ${H_1}^+$, by the relation

$${H_1}^-(z_0,t,t_0) = G^-(z_0,z_0,t,t_0) + \int_{t_0}^{t} G^-(z_0,z_0,t,t'){H_1}^+(z_0,t',t_0)\,dt'$$

3 The numerical implementation

One complication in the numerical implementation is that in (2.1) the slowness function $f(z,t)$ varies in both time and space. In algorithms based on hyperbolic equations, the characteristic curves are crucially coupled to the discretization mesh. The derivatives of the two families of characteristic curves $t = \tau^{\pm}(z;z_0,t_0)$, associated with the equations in (2.1) are

$$\frac{\mathrm{d}\tau^{\pm}}{\mathrm{d}z}(z;z_0,t_0) = \pm f(z,\tau^{\pm}(z;z_0,t_0))$$

This means that in general the characteristic curves are not straight. In principle, as can be seen in Ref. 3, appendix A, it is always possible to transform a problem with curved characteristics, into one with straight characteristics. The solution to this transformation is, however, of the same complexity as the original problem, and therefore not tractable. The well-known travel time transformation in one spatial dimension is one managable exception. The numerical implementation presented in this paper assumes that the slowness $f(z,t) = 1$, and that the thickness is normalized to $d = 1$. The latter restriction is no loss of generality.

Another complication is that the choice of discretization mesh in the integrals (2.2) is tied up by the meshgrid in the preceding calculation of the propagator kernels $G^{\pm}$ and $Q^{\pm}$. The same number of discretization intervals in z and z_0 was chosen when the final values of $u(z,t)$ were calculated, as was used for the propagator

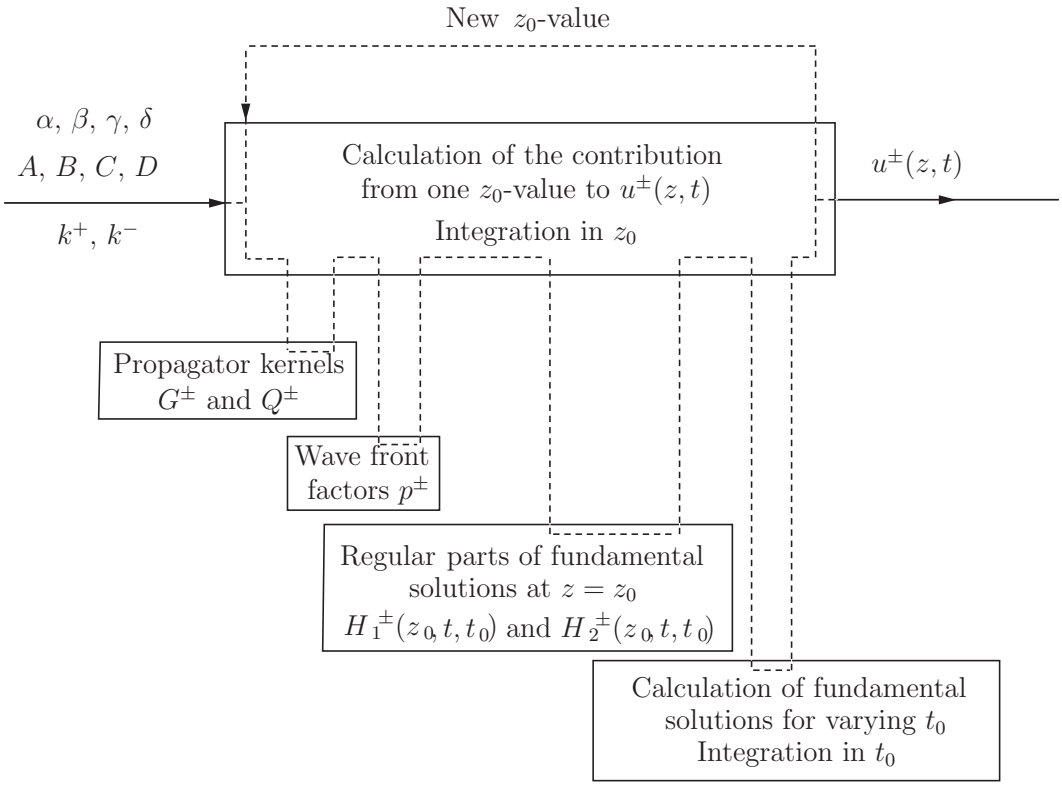

Figure 3: Organization of the data flow.

kernels. A nuisance is that $G^\pm$ and $Q^\pm$ are only known for the double step size in t_0. Therefore, for every second value of z_0, the endpoint $t_0 = \tau^\pm(z_0; z, t)$ of the t_0-integrals occurs in a point, where the fundamental solutions $E_1{}^\pm$ and $E_2{}^\pm$ are hard to evaluate. This was solved by interpolation which means some loss in accuracy. The alternative is to use only every second of the mesh-points in z and z_0 in the final calculation of $u(z,t)$, thus avoiding the unknown points. It is believed that the first alternative, although more cumbersome, is the more efficient way to obtain an accurate solution $u(z,t)$.

A rough outline of how the flow of data is organized, can be found in Figure 3. The central task of the code is to calculate the integrals (2.2). The minimum data input consists of six two-dimensional data fields containing the source functions $k^\pm$ and the coefficient functions α, β, γ and δ of the dynamics (2.1). The three-variable functions A, B, C and D are problematic. They simply take up too much memory, if they are stored in three-dimensional data-fields ahead of entering the main program. Despite an increase in the processing time, it may be more convenient to evaluate A, B, C and D as functions, every time they are called for. The decision how to handle A, B, C and D has to be taken for every problem separately. The output data $u^\pm(z,t)$ is stored in two-dimensional data fields. The calculations include the performance of many integrals. Throughout, the trapezoidal rule has been chosen. Now, the focus will be on the ideas behind some of the squares in Figure 3.

Integration in z_0.

The title refers to the integrals (2.2). The experience from the numerical work published in Ref. 2 suggested that special care had to be taken for the computer memory to suffice. In Ref. 2, the propagator kernels $G^{\pm}(z_0, z, t, t_0)$ were calculated for a semi-infinite medium. The waves originated solely from external sources, so only one value of z_0 was of interest, i.e. the boundary value $z_0 = 0$. The largest data fields required were three-dimensional. In the present case, with sources in the interior of the medium, all four parameters vary, since the z_0-values have to be chosen throughout the slab. Similarly, the fundamental solutions, ${E_1}^{\pm}$ and ${E_2}^{\pm}$, have four different parameters. A strategy to avoid four-dimensional fields had to be elaborated! The propagator equations in Ref. 1, Appendix A, show that in order to keep away from time-consuming repetitions, it is necessary to calculate the propagator kernels for all values of z and t sequentially. Another restriction becomes evident, when the integrals in the expressions (2.5) and (2.6) of the fundamental solutions ${E_1}^{\pm}$ are studied. Here, propagator kernels for varying t_0-values are needed simultaneously. The plan is therefore to calculate the contributions to $u^{\pm}(z, t)$ for all z and t from one z_0-value at a time. After finishing one z_0-calculation, the three-dimensional fields containing the propagator kernels $G^{\pm}$ and $Q^{\pm}$ and the two-dimensional fields containing the wave front factors $p^{\pm}$ and the regular parts of the fundamental solutions ${E_1}^{\pm}$ and ${E_2}^{\pm}$ can be erased, and thus be ready for reuse, when the next z_0-value is entered.

The propagator kernels $G^{\pm}$ and $Q^{\pm}$

Each pair of propagator kernels $G^{\pm}(z_0, z, t, t_0)$ and $Q^{\pm}(z_0, z, t, t_0)$ satisfy a coupled first order system of hyperbolic integro-differential equations with derivatives in z and t only, see Ref. 1, appendix A. Therefore, for every choice of z_0, the kernels can be calculated for one $t_0 = \textit{constant}$ -plane at a time. Initial values of G^- and Q^+ are given at $t = t_0$, homogeneous boundary values of G^+ and Q^- at $z = z_0$, and of Q^+ at $z = 0$ and G^- at $z = d$, respectively.

Each propagator equation is integrated along the characteristic curve. The integrals are first approximated using the trapezoidal rule, and then discretized in the remaining variables. At each mesh point, the two coupled equations are solved simultaneously. The details of the discretization and the computational molecule are similar to those of the direct algorithm of the Green functions equations in a semi-infinite medium, see Ref. 2. However, some new features should be mentioned:

Observe that the kernels $Q^{\pm}$ are defined in $0 < z < z_0$ and $G^{\pm}$ in $z_0 < z < d$, with z_0 moving through the interval $(0, d)$ between the successive calls. Therefore, it is convenient to store Q^+ and G^+ in one common data field with fixed limits. Similarly, Q^- and G^- can be stored together.

For each $t_0 = \textit{constant}$ -plane, the calculation starts at $t = t_0$. The time variable t is increased successively. For each choice of t, the calculation starts at $z = z_0$, and the propagator kernels $G^{\pm}$ are obtained after successive increments in z, until the boundary $z = d$ is reached. In the same manner, for $Q^{\pm}$ the calculation starts at $z = z_0$, and z is decreased until $z = 0$ is reached.

For the kernel G^-, a discontinuity may under certain conditions be introduced at the point $(z,t) = (d,t_0)$ of each $t_0 = \textit{constant}$ -plane, see Refs 1, 3. Likewise, the kernel Q^+ may have a discontinuity originating from $(z,t) = (0,t_0)$. The discontinuities propagate along the characteristic curves of the G^-- and Q^+-equations, respectively. Therefore, for each choice of t, as the characteristic curves are passed, the values of the discontinuities must be calculated and added to the relevant kernel functions.

The jumps in G^- and Q^+ call for even more attention. For all mesh-points located above the curves of discontinuity, the propagator equations have time-integrals extending across these curves. Thus, special care must be taken in performing these integrals.

Integration in t_0.

This item concerns the calculation of the fundamental solutions ${E_1}^{\pm}$, see the expressions (2.5)–(2.6), as well as the t_0-part of the double integrals (2.2), and the similar calculations leading to the solutions ${u_2}^{\pm}(z,t)$. The unknown endpoints of every second t_0-integral have already been mentioned. Upon the evaluation of the expressions (2.5)–(2.6), the problem is encountered again. To give a couple of examples, in (2.5) consider the functions $G^+(z_0,z,\tau^+(z_0;z,t),t_0)$ and ${H_1}^+(z_0,\tau^+(z_0;z,t),t_0)$. Here, t_0 is always an even multiple of the discretization interval in z_0, while $\tau^+(z_0;z,t)$ may be even or odd, depending on whether the distance between z and z_0 occupies an even or an odd number of discretization intervals. Similarly, the integrands of the integrals in (2.5) may be hard to evaluate at the end points $\tau^+(z_0;z,t)$. The algorithm of the propagator equations, which only permits the two time variables of $G^{\pm}$ and $Q^{\pm}$ to be even or odd simultaneously, also sets the constraints for the regular parts of the fundamental solutions at $z = z_0$, i.e. ${H_1}^{\pm}(z_0,t,t_0)$ and ${H_2}^{\pm}(z_0,t,t_0)$. Interpolation solves these problems, but they certainly make the code more complicated and harder to overlook.

4 Examples

In this section, two illustrative examples are presented. The calculations have been performed with the method summarized above.

The first example deals with wave propagation from internal sources in a Klein-Gordon medium. This specific problem has been chosen, because of the possibility to compare the result with an alternative solution, obtained by another, partially analytical technique. Therefore, the discussion in Example 1 starts with a presentation of the alternative method. It is shown that the solution calculated with the method of the previous sections, converges to the solution obtained by the alternative method, as the square of the used interval of discretization.

The purpose of the second example is to demonstrate the potential of the new method. It can be applied to problems, which have proven difficult to solve with conventional methods. Relevant examples can be found within a variety of technical applications. Here, the emphasis is on electrical engineering, and then especially on

the transmission line. Its properties have been chosen to demonstrate that rapid time variations can be modeled by the time dependent functions α, β, γ and δ, and A, B, C and D. Imaginatively, these time variations have been provoked by a thunderstorm!

4.1 Example 1

The starting point is the one-dimensional Klein-Gordon equation

$$\frac{\partial^2}{\partial z^2}u(z,t) - \frac{1}{c^2}\frac{\partial^2}{\partial t^2}u(z,t) - \kappa^2 u(z,t) = g(z,t)\,, \quad z \in [0,d] \tag{4.1}$$

valid in the medium inside the slab $0 \le z \le d$. The phase velocity c of the wave has a constant, positive value, the same as in the surrounding medium. The real parameter κ is related to the elasticity of the medium, and the function $g(z,t)$ is the source function. The regions $z < 0$ and $z > d$ are free space, so the corresponding wave equation is

$$\frac{\partial^2}{\partial z^2}u(z,t) - \frac{1}{c^2}\frac{\partial^2}{\partial t^2}u(z,t) = 0\,, \quad z < 0, z > d \tag{4.2}$$

It is easy to show that the solution u of this problem, as given in Ref. 1, is continuously differentiable in z everywhere, including the end points of the slab at $z = 0$ and $z = d$. This property is insured by the continuity of the wave phase velocity c for all z.

For a moment, consider an infinite Klein-Gordon medium, with sources in the region $0 \le z \le d$. In Ref. 27, p. 475, the solution of the initial value problem for an infinite Klein-Gordon medium, with equation (4.1) valid for all z, is discussed. With homogeneous initial conditions

$$u(z,0) = 0, \qquad \frac{\partial}{\partial t}u(z,0) = 0, \qquad -\infty < z < \infty$$

and with the source function $g(z,t)$ supported in the region $0 \le z \le d$ and $t \ge 0$, the solution for $t \ge 0$ is

$$\begin{cases} u(z,t) = -\dfrac{c}{2}\displaystyle\int_0^z \left\{ \int_0^{\frac{1}{c}(z_0-z)+t} J_0\left(\kappa\sqrt{c^2(t-t_0)^2-(z-z_0)^2}\right) g(z_0,t_0)\,dt_0 \right\} dz_0 \\ \qquad -\dfrac{c}{2}\displaystyle\int_z^d \left\{ \int_0^{-\frac{1}{c}(z_0-z)+t} J_0\left(\kappa\sqrt{c^2(t-t_0)^2-(z-z_0)^2}\right) g(z_0,t_0)\,dt_0 \right\} dz_0 \end{cases} \tag{4.3}$$

in $0 \le z \le d$, and

$$u(z,t) = -\frac{c}{2}\int_0^d \left\{ \int_0^{t-\frac{1}{c}|z-z_0|} J_0\left(\kappa\sqrt{c^2(t-t_0)^2-(z-z_0)^2}\right) g(z_0,t_0)\,dt_0 \right\} dz_0 \tag{4.4}$$

in the regions $z < 0$ and $z > d$. Here, J_0 is the Bessel function of the first kind of order zero. Observe that the factor

$$-\frac{c}{2}J_0\left(\kappa\sqrt{c^2(t-t_0)^2-(z-z_0)^2}\right)H(t-t_0-\frac{1}{c}|z-z_0|) \tag{4.5}$$

is the fundamental wave response of an excitation from a point source $\delta(z-z_0)\delta(t-t_0)$ at the space-time point (z_0, t_0). Note, the Heaviside step function $H(t)$.

In Figures 4–6, the solution $u(z,t)$, given by (4.3), is shown for $0 \le z \le d$, and $0 \le t \le 2.25$, for three different angles of observation. In this calculation the thickness d has been chosen as 1 unit of length, and the phase velocity c is 1 unit of speed. These choices introduce no restrictions, since unit values can always be attained by means of an elementary travel time coordinate transformation, see e.g. Ref. 2. The time interval of the calculation, 2.25, is long enough for waves excited at the starting time $t = 0$, to travel more than one full round trip through the slab. The parameter κ has been chosen as $\kappa = 5.0$, and the source function is

$$g(z,t) = \begin{cases} \cos(\pi z)\sin(10t), & 0 \le z \le d, \quad t \ge 0 \\ 0, & z \le 0, \ \ z \ge d, \quad t \ge 0 \\ 0, & -\infty < z < \infty, \quad t < 0 \end{cases} \tag{4.6}$$

The number of mesh-intervals is 64×144. Especially, notice the behaviour close to the boundaries $z = 0$ and $z = d$, and in Figure 6, note the attenuation of the solution at $t = 1.7$, a point of time, which coincides with the third minimum of the Bessel function J_0 for waves initiated at $t = 0$.

The solution (4.3)–(4.4) assumes that the Klein-Gordon equation holds everywhere in space, $-\infty < z < \infty$. To handle the problem of equations (4.1)–(4.2), where the Klein-Gordon equation holds only inside the slab $0 < z < d$, the solution (4.3)–(4.4) has to be modified. This modification is now considered.

The approach to solve this problem relies on a method to treat transient electromagnetic wave propagation in waveguides [16], but the method is also applicable to the present problem. For convenience, some of the results of Ref. 16 are repeated here:

Consider the transformation K, given by

$$\begin{pmatrix} u^+ \\ u^- \end{pmatrix} = \frac{1}{2}\begin{pmatrix} 1 & -cK \\ 1 & cK \end{pmatrix}\begin{pmatrix} u \\ \partial_z u \end{pmatrix} \tag{4.7}$$

The operator K has the integral representation

$$(Kf)(t) = \int_{-\infty}^{t} J_0(c\kappa(t-t'))f(t')dt'$$

By this transformation, the dependent variable u of the Klein-Gordon equation (4.1) is split into the two components u^+ and u^-. The inverse transformation K^{-1} is given by

$$\begin{pmatrix} u \\ \partial_z u \end{pmatrix} = \begin{pmatrix} 1 & 1 \\ -\frac{1}{c}K^{-1} & \frac{1}{c}K^{-1} \end{pmatrix}\begin{pmatrix} u^+ \\ u^- \end{pmatrix} \tag{4.8}$$

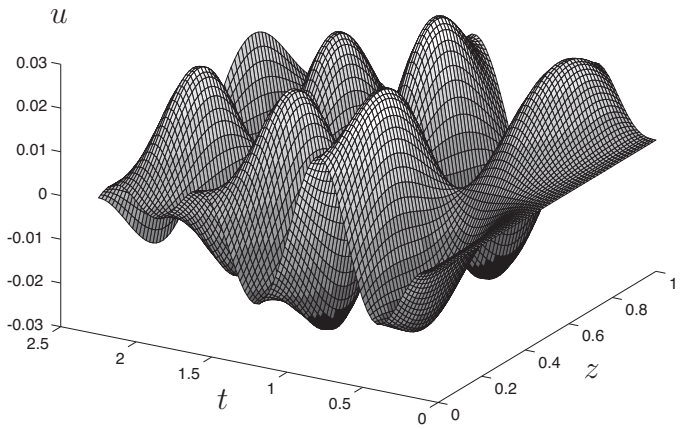

Figure 4: Waves in an infinite Klein-Gordon medium—View 1.

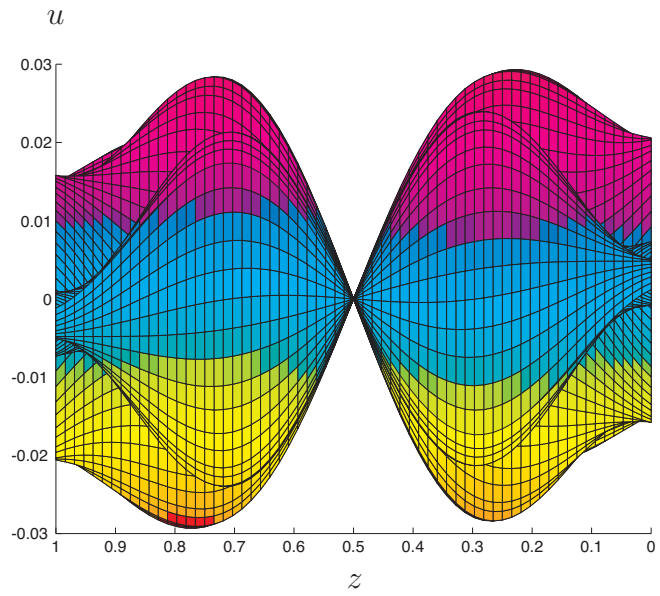

Figure 5: Waves in an infinite Klein-Gordon medium—View 2.

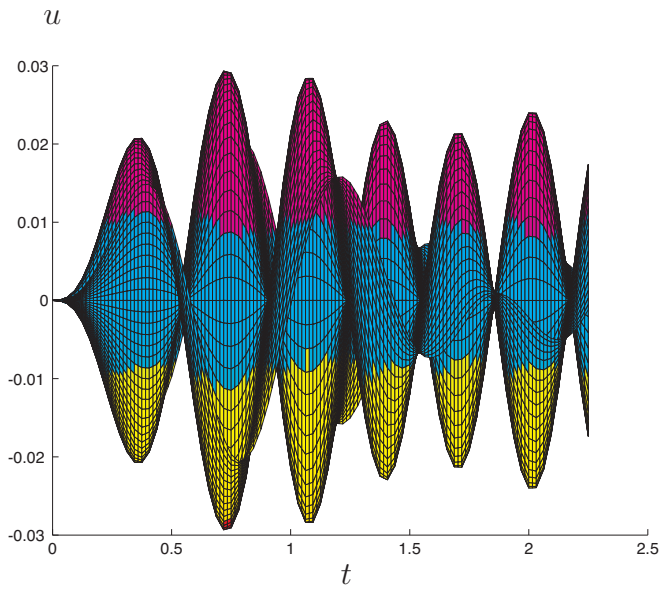

Figure 6: Waves in an infinite Klein-Gordon medium—View 3.

The inverse operator K^{-1} has the integral representation

$$(K^{-1}f)(t) = \frac{\partial f}{\partial t} + c\kappa \int_{-\infty}^{t} \frac{J_1(c\kappa(t-t'))}{t-t'} f(t')dt' \tag{4.9}$$

The Klein-Gordon wave splitting transformation (4.7) is ideal, since equation (4.1) is transformed into a set of uncoupled first order equations in $u^{\pm}$.

$$\frac{\partial}{\partial z}\begin{pmatrix} u^+ \\ u^- \end{pmatrix} = \begin{pmatrix} -\frac{1}{c}K^{-1} & 0 \\ 0 & \frac{1}{c}K^{-1} \end{pmatrix}\begin{pmatrix} u^+ \\ u^- \end{pmatrix} \tag{4.10}$$

The diagonal configuration of (4.10) shows that the two wave components u^+ and u^- have a deeper physical significance, than just being mathematical quantities. The wave component u^+ is a wave, which travels to the right, and u^- is a left-going wave. The condition

$$\frac{\partial}{\partial z}u(z,t) = \mp\frac{1}{c}\left(K^{-1}u(z,\cdot)\right)(t) \tag{4.11}$$

can be used to test, if a wave field u is identical to only one of the components u^+ or u^-. The upper sign equality is satisfied by right-going fields, and the lower one by left-going fields. The relations (4.7) – (4.11) contain most of the information needed to modify the solution (4.3)–(4.4) into the solution of problem (4.1)–(4.2).

In $z < 0$, the waves given by (4.4) are true left-traveling waves. This is so, because the waves originate from sources situated in $0 \le z \le d$. For similar reasons, the waves given by (4.4) in the region $z > d$ are true right-going waves. When applied to the waves (4.4), the condition (4.11) is equivalent to the following identity of Bessel functions:

$$(x-\alpha)\frac{J_1\left((x^2-\alpha^2)^{\frac{1}{2}}\right)}{(x^2-\alpha^2)^{\frac{1}{2}}} = \int_{\alpha}^{x} \frac{J_1(x-y)}{x-y} J_0\left((y^2-\alpha^2)^{\frac{1}{2}}\right) dy\,, \quad x,\alpha \in \mathbb{C} \tag{4.12}$$

which can be proved by Laplace transform techniques. If (4.11) is applied directly to the fundamental waves (4.5), it is found that (4.5) models a right-going wave for $z > z_0$ and a left-going one for $z < z_0$. Again, the condition (4.11) is equivalent to the Bessel identity (4.12).

Another consequence of (4.11) is that neither one of the two terms of the wave field (4.3) can be found to be completely identical to a right- or a left-going wave. The independent variable z, appearing as a limit in the first integral symbol of each of the terms, causes additional terms in the z-derivatives, compared to the corresponding derivatives of (4.4). In (4.11) these terms remain unbalanced, whereas the rest of the terms again cancel by (4.12).

Instead, consider the total wave field $u(z,t)$ in (4.3). For almost all space points within the slab, the wave field $u(z,t)$ is a mixture of right- and left-going wave fields. However, if (4.11) is applied to the full expression in (4.3), it can be seen that in the limit, as $z \to 0+$, all integral components derived from the first term in (4.3) disappear, so only the z-derivative term mentioned above remains. It is canceled by the corresponding z-derivative term derived from the second term in (4.3). The rest

of the terms cancel by (4.12). Therefore (4.3) models a leftgoing wave at $z = 0+$. Vice versa, (4.3) models a right-going wave at $z = d-$.

Now, return to the problem (4.1)–(4.2) with sources in a Klein-Gordon slab surrounded by free space. Outside of the slab, in free space, the complete wave splitting which diagonalizes the wave equation (4.4) is given by

$$\begin{pmatrix} u^+ \\ u^- \end{pmatrix} = \frac{1}{2} \begin{pmatrix} 1 & -c\partial_t^{-1} \\ 1 & c\partial_t^{-1} \end{pmatrix} \begin{pmatrix} u \\ \partial_z u \end{pmatrix} \tag{4.13}$$

The anti-derivative is defined as

$$\partial_t^{-1} g(t) = \int_{-\infty}^{t} g(t')dt'$$

The inverse of (4.13) is

$$\begin{pmatrix} u \\ \partial_z u \end{pmatrix} = \begin{pmatrix} 1 & 1 \\ -\frac{1}{c}\partial_t & \frac{1}{c}\partial_t \end{pmatrix} \begin{pmatrix} u^+ \\ u^- \end{pmatrix} \tag{4.14}$$

In this paper it is assumed that there are no sources exterior to the slab. Therefore, for the problem (4.1)–(4.2), at $z = 0$ the boundary condition

$$u^+(0-, t) = 0 \tag{4.15}$$

is valid together with the conditions of continuity

$$\begin{cases} u(0-, t) = u(0+, t) \\ \dfrac{\partial u}{\partial z}(0-, t) = \dfrac{\partial u}{\partial z}(0+, t) \end{cases} \tag{4.16}$$

The inverse transformation (4.14) together with (4.15) show that

$$\frac{\partial u}{\partial z}(0-, t) = \frac{1}{c}\frac{\partial u^-}{\partial t}(0-, t)$$

Therefore, if

$$u(0+, t) \quad \text{and} \quad \frac{\partial u}{\partial z}(0+, t)$$

are substituted using the inverse Klein-Gordon transformation (4.8), the boundary conditions (4.16) turn into

$$\begin{cases} u^-(0-, t) = u^+(0+, t) + u^-(0+, t) \\ \dfrac{\partial u^-}{\partial t}(0-, t) = -K^{-1}u^+(0+, t) + K^{-1}u^-(0+, t) \end{cases} \tag{4.17}$$

Elimination of

$$\frac{\partial u^-}{\partial t}(0-, t)$$

and the use of (4.9) yield

$$\begin{aligned} 2\frac{\partial u^+}{\partial t}(0+,t) + c\kappa \int_{-\infty}^{t} \frac{J_1\left(c\kappa(t-t')\right)}{t-t'} u^+(0+,t')dt' \\ = c\kappa \int_{-\infty}^{t} \frac{J_1(c\kappa(t-t'))}{t-t'} u^-(0+,t')dt' \end{aligned} \tag{4.18}$$

From this equation the reflected boundary wave $u^+(0+,t)$ can be calculated. The field $u^-(0+,t)$ is partially known. It is given by $u(z,t)$ in (4.3), evaluated at $z=0$, for non-reflected waves impinging directly from the source.

A similar relation, can be derived at $z=d$. It is

$$\begin{aligned} 2\frac{\partial u^-}{\partial t}(d-,t) + c\kappa \int_{-\infty}^{t} \frac{J_1(c\kappa(t-t'))}{t-t'} u^-(d-,t')dt' \\ = c\kappa \int_{-\infty}^{t} \frac{J_1\left(c\kappa(t-t')\right)}{t-t'} u^+(d-,t')dt' \end{aligned} \tag{4.19}$$

Here $u^+(d-,t)$ is given by (4.3), evaluated at $z=d$. From (4.19), $u^-(d-,t)$ can be reconstructed.

One advantage, using the concept of wave splitting, is that propagators can be used to advance boundary waves into the interior of the slab. The following expressions, which are obtained from Duhamel's integral, see e.g. Refs 3, 12, 16, show how the right-going boundary wave component $u^+(0+,t)$ is propagated:

$$\begin{cases} u^+(z,t+\dfrac{z}{c}) = u^+(0+,t) + \displaystyle\int_{-\infty}^{\infty} G^+(z,t-t')u^+(0+,t')dt' \\ u^-(z,t+\dfrac{z}{c}) = 0 \end{cases} \tag{4.20}$$

with

$$G^+(z,t) = -c\kappa z H(t) \frac{J_1\left(\kappa\sqrt{c^2t^2+2zct}\right)}{\sqrt{c^2t^2+2zct}}$$

Note, the Heaviside step function $H(t)$. Similar expressions for propagation of the left-going boundary wave $u^-(d-,t)$ are

$$\begin{cases} u^-(z,t+\dfrac{d-z}{c}) = u^-(d-,t) \\ \qquad\qquad - c\kappa(d-z)\displaystyle\int_{-\infty}^{t} \frac{J_1\left(\kappa\sqrt{c^2(t-t')^2+2(d-z)c(t-t')}\right)}{\sqrt{c^2(t-t')^2+2(d-z)c(t-t')}} u^-(d-,t')dt' \\ u^+(z,t+\dfrac{d-z}{c}) = 0 \end{cases} \tag{4.21}$$

The relations (4.18)-(4.21) are the tools needed to modify the wave field (4.3) to solve the Klein-Gordon equation (4.1) in the interior of a slab in position $(0,d)$, surrounded by free space. The expression (4.3) is still valid, but only for waves

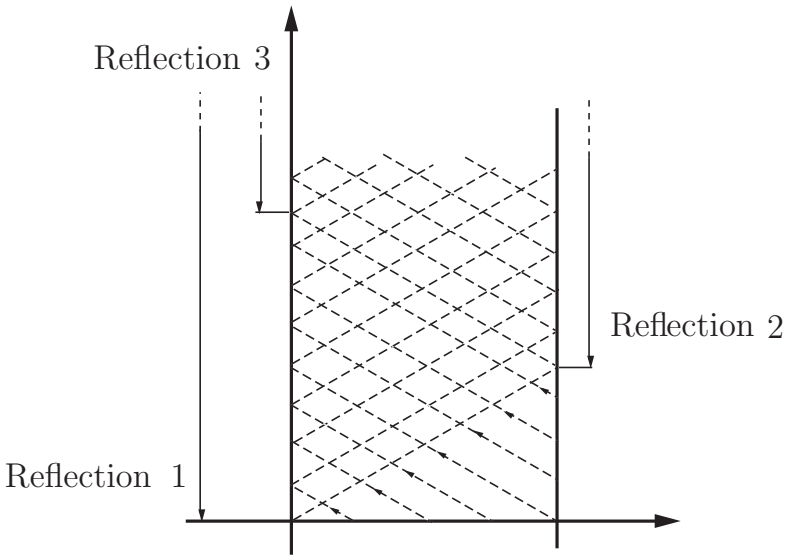

Figure 7: The reflection pattern of initially left-going waves.

coming directly from the source, up to the moment they encounter the boundary at $z = 0$ or $z = d$. There, they are reflected, and the reflected waves can be calculated from the formulas (4.18)–(4.21). When the so reflected waves arrive at the opposite boundary, they are reflected a second time .... Repeated use of the formulas (4.18)–(4.21) is therefore necessary. Figure 7 shows the pattern of reflection for waves initially propagating to the left. For the time interval 2.25 used in this example, a number of three sequential reflections have to be considered. The desired solution to the problem (4.1)–(4.2) is obtained by adding all reflected wave fields to the solution (4.3).

In the problem illustrated by the Figures 4–6, the slab-like region $(0, d)$ is part of an infinite Klein-Gordon medium. Then the solution for $z < 0$ and $z > d$ is given by expression (4.4). The Figures 8–10 show the corresponding solution of the problem (4.1)–(4.2). The choice of parameters (κ,c,d), source function and number of mesh-intervals are the same, as in the calculations of the Figures 4–6. In the surrounding medium, free space, the wave solutions can easily be deduced from the boundary values $u(0, t)$ and $u(d, t)$. They are

$$u(z,t) = \begin{cases} u(0, t + \dfrac{z}{c}), & z < 0 \\ u(d, t + \dfrac{d-z}{c}), & z > d \end{cases}$$

The Figures 8–10 show the waves calculated with the methods given in Ref. 1. If the transformation (4.13) is applied to the Klein-Gordon equation (4.1), the coefficient functions of the dynamics (2.1) are found to be $\alpha(z, t) = \beta(z, t) = \gamma(z, t) = \delta(z, t) = 0$ and $A = B = C = D = -\frac{1}{2}\kappa^2$. The single source function (4.6) is for $0 \le z \le d$ and $t \ge 0$ transformed into the doublet

$$k^{\pm}(z,t) = \mp 0.05 \cos(\pi z)\,(1 - \cos(10t))$$

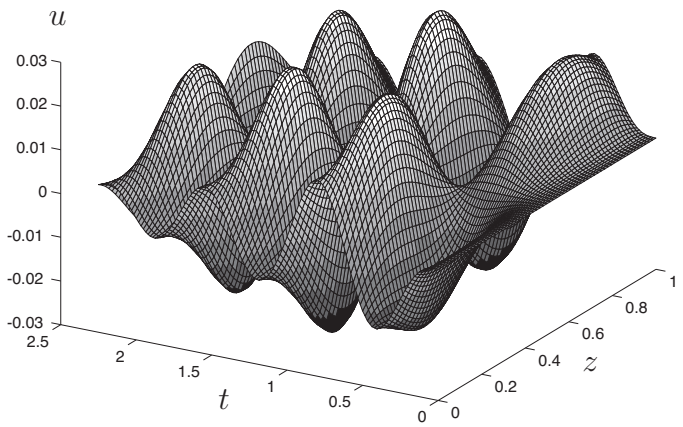

Figure 8: Waves in a Klein-Gordon slab surrounded by free space—View 1.

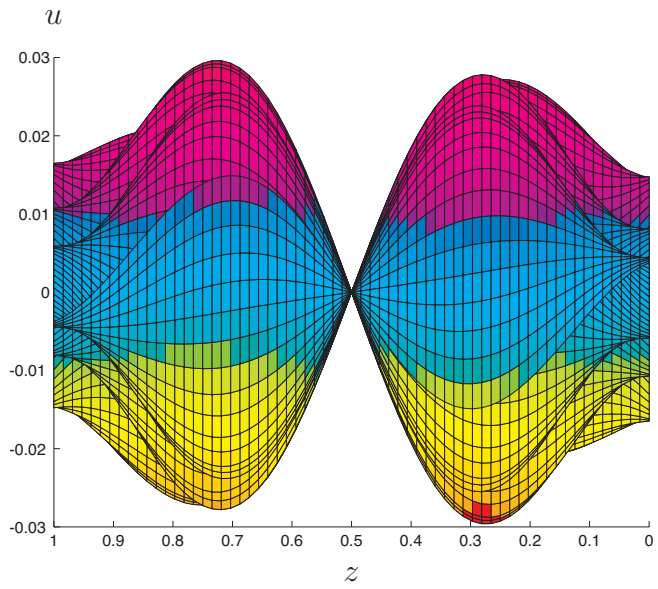

Figure 9: Waves in a Klein-Gordon slab surrounded by free space—View 2.

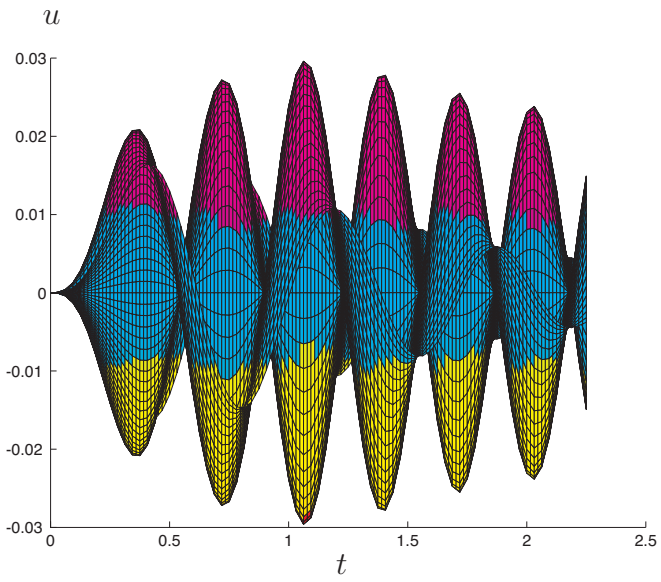

Figure 10: Waves in a Klein-Gordon slab surrounded by free space—View 3.

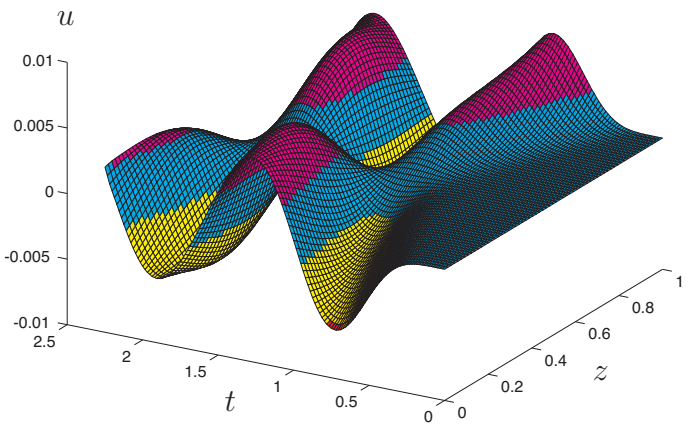

Figure 11: The difference between the two wave solutions.

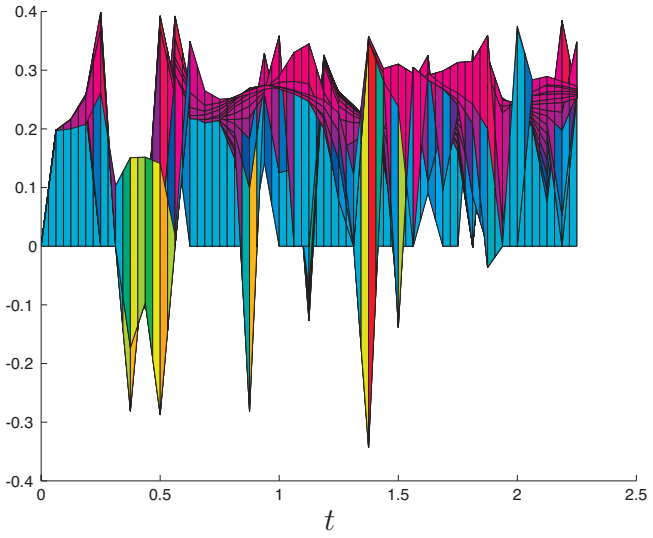

Figure 12: The error quotient.

Calculations performed with the alternative method, i.e. the wave solution (4.3) modified with the expressions (4.18)-(4.21) for reflections at the slab boundaries, give results indistinguishable at the scale shown in Figures 8–10.

If the Figures 8–10 are compared to the Figures 4–6 some differences are easily recognized. One of them is the reduced range of the wave field at the boundaries $z = 0$ and $z = d$. Another observation is that the attenuation in u at $t = 1.7$ has disappeared. Instead, Figure 10 shows that the maximum values of the oscillations decrease gradually. In order to make the comparison easier, the difference between the two wave fields in the Figures 8 and 4 is shown in Figure 11.

The method presented in Ref. 1 is very general, and can be applied to a wide variety of problems. The alternative method presented above can be used only for sources in a Klein-Gordon slab. The special attention, which has been paid to it in this paper, is motivated by the fact that it provides a way to verify the results of the general method for this particular example. Figure 12 illustrates the outcome of the comparison:

First a wave field was calculated with the alternative method. The choice of the number of mesh-intervals was 128×288. This wave solution was used as a normal. Then the calculation was repeated twice, with two different choices of mesh-intervals , 64×144 and 32×72, now using the method of Ref. 1. The errors, i.e. the difference between each of the solutions performed with the general method, and the normal, were calculated. With the finer mesh (64×144) the range of the errors was $\mid \triangle u \mid \leq 1.5 \times 10^{-4}$, and with the coarser mesh (32×72) the range was $\mid \triangle u \mid \leq 6 \times 10^{-4}$. For every mesh-point of the coarser mesh, the quotient of the two errors, obtained with the finer and coarser meshes, was calculated. In order to better estimate the average value, all points with quotients > 0.4 were excluded from Figure 12. This means that 164 of the total 1221 points, i.e. 13.4%, are not represented in Figure 12. As can be seen, the average absolute value of the error quotient is very close to 0.25. In fact, 700 points (57%) have error quotients in the range 0.2–0.3. The remainder of the 1221 points are distributed evenly around this interval, 22% above and 21% below. A special investigation was performed for the excluded points. It was found that 28 points (2.5%) have error quotients > 2, and 76 points (6%) have error quotients > 1. For all of these, seemingly non-converging points, it proved that the error in the coarse calculation was $< 10^{-5}$, for most of them even $< 10^{-6}$. For the rest of the excluded points, with quotients in the interval 0.4–1, the error of the coarser calculation was still very small, close to 10^{-5}. Therefore, considering that the calculations were performed with single precision, for the excluded points with the finer choice of mesh, it can be infered that the disability of the computer to represent small numbers has dominated over the truncation errors. The conclusion is that for non-converged points, the average error quotient is 0.25. Therefore, put in other words, for this particular example, the calculations performed with the general method of Ref. 1, in average converge to the "true" solution, here calculated with the alternative method, as the square of the used interval of discretization.

4.2 Example 2

An open circuit, two-wire transmission line, with length $d = 10$ km, is studied. The current and voltage waves generated by the normal line supply at one end, can easily be evaluated with the methods of Ref. 3, see also [20]. Instead, waves originating from internal current and voltage sources are calculated, see Figure 13. Imaginatively, a thunder cloud piles up at the central part (1 km) of the transmission line, and the lightning, modeled by the sources $I_0(z,t)$ and $V_0(z,t)$, strikes the line. The transmission line equations are given by Ref. 3

$$\begin{pmatrix} 0 & C(z,t) \\ L(z,t) & 0 \end{pmatrix} \frac{\partial}{\partial t} \begin{pmatrix} i(z,t) \\ v(z,t) \end{pmatrix} + \frac{\partial}{\partial z} \begin{pmatrix} i(z,t) \\ v(z,t) \end{pmatrix} - B \begin{pmatrix} i(z,t) \\ v(z,t) \end{pmatrix} = \begin{pmatrix} I_0(z,t) \\ V_0(z,t) \end{pmatrix} \tag{4.22}$$

where the operator matrix B is given by

$$B = \begin{pmatrix} 0 & -G(z,t) - \frac{\partial C}{\partial t}(z,t) - \frac{\partial}{\partial t} \int_{-\infty}^{t} \chi_e(z,t,t') \bullet dt' \\ -R(z,t) - \frac{\partial L}{\partial t}(z,t) - \frac{\partial}{\partial t} \int_{-\infty}^{t} \chi_m(z,t,t') \bullet dt' & 0 \end{pmatrix}$$

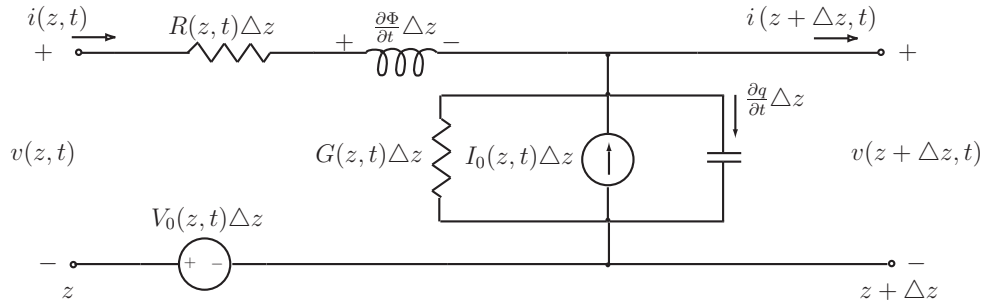

Figure 13: Internal sources on the transmission line.

The symbol $\bullet$ denotes the place holder for the operand. In these equations, $R(z,t)$ and $G(z,t)$ are the series resistance and the shunt conductance per unit length of the transmission line, respectively. The series inductance and the shunt capacitance per unit length, denoted $L(z,t)$ and $C(z,t)$, respectively, are assumed positive and finite. The voltage $v(z,t)$ and the current $i(z,t)$ are related, respectively, to the magnetic flux $\Phi(z,t)$ and the charge $q(z,t)$ through

$$\begin{cases} \Phi(z,t) = L(z,t)i(z,t) + \displaystyle\int_{-\infty}^{t} \chi_m(z,t,t')i(z,t')\,dt' \\ q(z,t) = C(z,t)v(z,t) + \displaystyle\int_{-\infty}^{t} \chi_e(z,t,t')v(z,t')\,dt' \end{cases} \tag{4.23}$$

The magnetic flux, $\Phi(z,t)$, and the electric charge, $q(z,t)$, depend on the current $i(z,t)$ and the voltage $v(z,t)$ at time t, respectively. In addition to these multiplicative terms, Φ and q are connected to the previous values of the currents and voltages of the transmission line. The memory functions are modeled by the two integral terms with the kernels $\chi_m(z,t,t')$ describing the inductive susceptibility and $\chi_e(z,t,t')$ modeling the capacitive susceptibility.

It has already been shown in Ref. 3 how these equations can be put on the form of (2.1). It is new that the right side of (2.1) is

$$\begin{pmatrix} k^+(z,t) \\ k^-(z,t) \end{pmatrix} = \frac{1}{2} \begin{pmatrix} I_0(z,t) + \sqrt{\frac{C(z,t)}{L(z,t)}} V_0(z,t) \\ I_0(z,t) - \sqrt{\frac{C(z,t)}{L(z,t)}} V_0(z,t) \end{pmatrix} \tag{4.24}$$

In the calculations presented here, the parameters have been chosen as

$$\begin{cases} R(z,t) = 0 \ \ (\Omega/\mathrm{m}) \\ L(z,t) = \mu_0 = 4\pi \cdot 10^{-7} \ \ (\mathrm{H/m}) \\ C(z,t) = \epsilon_0 \approx 8.854 \cdot 10^{-12} \ \ (\mathrm{F/m}) \\ \chi_m(z,t,t') = 0 \ \ (\mathrm{H/m{\cdot}s}) \end{cases}$$

The capacitive susceptibility χ_e is chosen as a Debye model. The expression given in (4.23) for the charge q of the shunt capacitance, has a parallel in the constitutive

relation connecting the electric displacement field $\boldsymbol{D}(\boldsymbol{r},t)$ to the electric field $\boldsymbol{E}(\boldsymbol{r},t)$:

$$\boldsymbol{D}(\boldsymbol{r},t) = \epsilon_0\epsilon(z,t)\boldsymbol{E}(\boldsymbol{r},t) + \int_{-\infty}^{t} \chi_e(z,t,t')\boldsymbol{E}(\boldsymbol{r},t')\,dt'$$

In Ref. 2, an expression for χ_e building on the Debye model was obtained. The underlying equation of the polarization vector is

$$\frac{\mathrm{d}\boldsymbol{P}}{\mathrm{d}t}(z,t) = \chi_0(z,t)\boldsymbol{E}(z,t) - \frac{1}{\tau(z,t)}\boldsymbol{P}(z,t) \tag{4.25}$$

The first term on the right hand side is the term responsible for the alignment effects in the medium ($\chi_0(z,t)$ is proportional to the alignment frequency), while the second term involving the relaxation time τ models the effect of random order. Together with the constitutive relation this yields

$$\begin{cases} \epsilon = 1 \\ \chi_e(z,t,t') = \chi_0(z,t')\exp\left\{-\displaystyle\int_{t'}^{t} \frac{dt''}{\tau(z,t'')}\right\} \end{cases}$$

Note that the choice of shunt capacitance $C(z,t) = \epsilon_0$ implies that $\epsilon = 1$. In the calculations presented in this example, the medium surrounding the transmission line is assumed homogeneous, so the spatial dependence in χ_e, χ_0 and τ disappears. Furthermore, it is assumed that χ_0 is independant of t'.

The results of the calculation are illustrated by the Figures 14–19. Observe that normalized coordinates x and s are used. With the suggested choices of parameters $L(z,t) = \mu_0$ and $C(z,t) = \epsilon_0$, the wave front velocity of the wave becomes the speed of light in vacuum $c_0 = 3 \cdot 10^8$ m/s. Therefore, the real space variable z and the time variable t are proportionally related to x and s by

$$\begin{cases} z = d\,x = 10^4 x \ \text{(m)} \\ t = ls = \dfrac{1}{3}10^{-4}s \ \text{(seconds)} \end{cases}$$

Note, the constant $l = \frac{d}{c_0}$. In the normalized time s, it takes the wave front 1 unit of time to pass from one end of the transmission line to the other end. If the relaxation time τ is expressed in normalized time coordinates, the susceptibility kernel is

$$\chi_e(sl, s'l) = \chi_0 \exp\left\{-\int_{s'}^{s} \frac{ds''}{\tau(s'')}\right\}$$

The choice of relaxation time function is the same as in Ref. 2:

$$\frac{1}{\tau(s)} = \begin{cases} \frac{1}{\tau_1}, & 0 \le s \le s_1 \\ \frac{\tau_1+\tau_2}{2\tau_1\tau_2} - \frac{\tau_1-\tau_2}{2\tau_1\tau_2}\cos\pi\frac{s-s_1}{s_2-s_1}, & s_1 \le s \le s_2 \\ \frac{1}{\tau_2}, & s_2 \le s \end{cases}$$

with $\tau_1 = 1$, $\tau_2 = 6$, $s_1 = 0.2$ and $s_2 = 1.4$. Notice that the alignment effect, represented by the first term in (4.25), gradually becomes dominant in the right

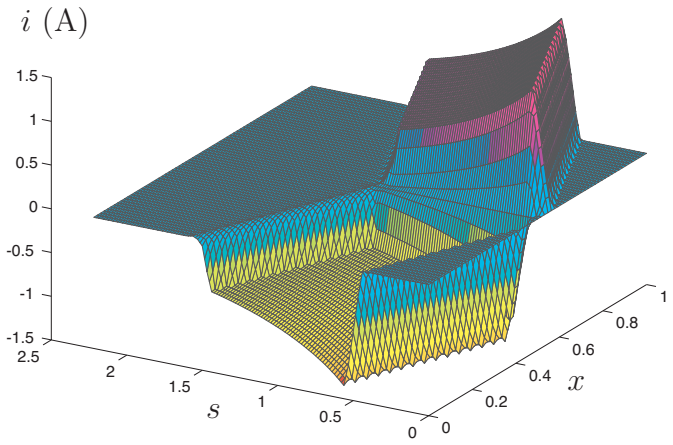

Figure 14: Current waves from current sources—$G_0 = 2.2 \cdot 10^{-5}$ and $\chi_0 = 0$.

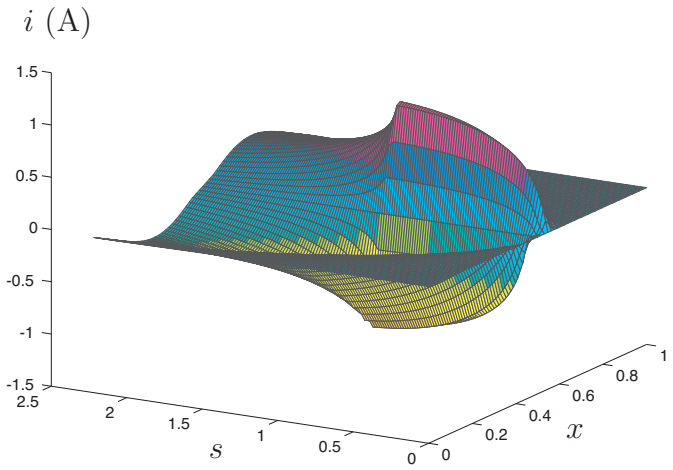

Figure 15: Current waves from current sources—$G_0 = 0$ and $\chi_0 = 2.2 \cdot 10^{-5}$.

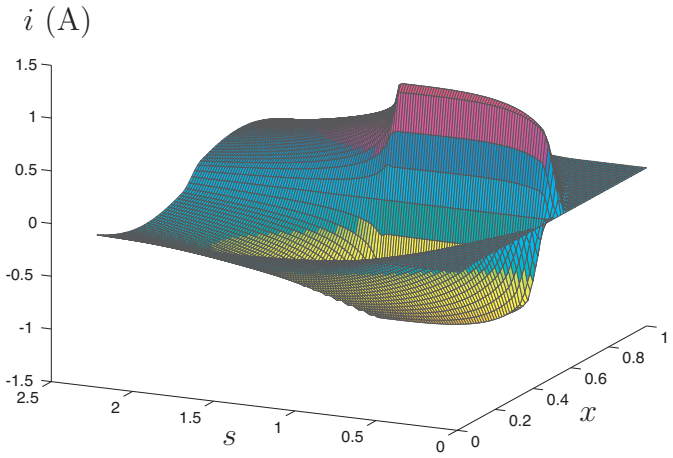

Figure 16: Current waves from current sources—$G_0 = 1.5{\cdot}10^{-5}$ and $\chi_0 = 0.7{\cdot}10^{-5}$.

side of (4.25). The shunt conductance $G(z,t)$ is chosen equal to zero outside the source region of the transmission line. In the middle tenth $4500 \leq z \leq 5500$ (m), i.e. the area of bad weather, the shunt conductance is an exponentially increasing function of time:

$$G(z,t) = G_0 \left(e^{0.5t} - 1\right) \sin(\pi(0.001z - 4.5)) \ \text{(S/m)}$$

Observe, the constant G_0. The explicit expressions of the coefficients in (2.1) are

$$\begin{cases} f(z,t) = \sqrt{LC} \\ \alpha(z,t) = \gamma(z,t) = -\dfrac{1}{2}\sqrt{\dfrac{L}{C}}\,[G(z,t) + \chi_0] \\ \beta(z,t) = \delta(z,t) = +\dfrac{1}{2}\sqrt{\dfrac{L}{C}}\,[G(z,t) + \chi_0] \end{cases}$$

and

$$\begin{cases} A(z,t,t') = C(z,t,t') = -\dfrac{1}{2}\sqrt{\dfrac{L}{C}}\dfrac{\partial \chi_e}{\partial t}(t,t') \\ B(z,t,t') = D(z,t,t') = +\dfrac{1}{2}\sqrt{\dfrac{L}{C}}\dfrac{\partial \chi_e}{\partial t}(t,t') \end{cases}$$

The lightning, represented by the source functions $I_0(z,t)$ and $V_0(z,t)$, only strikes the central part of the transmission line. In the Figures 14–19, only one kind of sources $I_0(z,t)$ or $V_0(z,t)$ is considered at a time. The sources are switched on at the normalized time $s = 0$, and stay constant until they are switched off at $s = 1$. Voltage sources are given by

$$V_0(xd, sl) = \begin{cases} 1 \ \text{(V/m)}, & 0.45 \leq x \leq 0.55, \ \ 0 \leq s \leq 1 \\ 0 \ \text{(V/m)}, & \text{for all other } x \text{ and } s \end{cases}$$

and current sources by

$$I_0(xd, sl) = \begin{cases} \sqrt{\dfrac{C}{L}} V_0 \approx 2.65 \ \text{(mA/m)}, & 0.45 \leq x \leq 0.55, \ \ 0 \leq s \leq 1 \\ 0 \ \text{(A/m)}, & \text{for all other } x \text{ and } s \end{cases}$$

Here, the constant $V_0 = 1$ V/m. Also, notice the linearity of the equations (2.1). In the Figures 14–19, this means that if the source functions I_0 or V_0 are multiplied by any factor, the observed currents and voltages are multiplied by the same factor.

The Figures 14–17 illustrate calculations for transmission lines with current sources only. The number of mesh-intervals is 128×288 in each calculation. In Figure 14, $G_0 = 2.2 \cdot 10^{-5}$ and $\chi_0 = 0$. Note that the current $i(x,s)$ is an odd function of x around $x = 0.5$. All along the transmission line, after a time determined by the position on the line and the velocity of the current wave front, the electric fields in the shunt capacitors and magnetic fields in the series inductors are built up. Since both χ_e and χ_m equal zero, there is no memory. Therefore voltages and

currents build up quickly. An experiment with $G_0 = 0$ everywhere, shows that the voltage and current in that case stay constant until the current sources have been shut off. With $G \neq 0$ in the central area, a counter-effect takes place. At the same time as the current sources provide new energy to the fields, there is a discharge through the shunt conductance. In Figure 14, this shows as a decrease in current prior to the sources being turned off. Also observe that due to the lack of memory, the final discharge is as abrupt as the build-up.

In Figure 15, the transmission line current is shown for a case with $\chi_0 = 2.2 \cdot 10^{-5}$ and $G_0 = 0$. Again electric and magnetic fields are built up, but this time very slowly, since the capacitors have memory. It can be seen from the last expression in (4.23) that with $\chi_e \neq 0$ a specific value of q implies a lower voltage, than would be the case with $\chi_e = 0$. A quick glance at Figure 15 hints that the wave front speed is slower than in Figure 14. However, this is an illusion. A close investigation shows that the voltage and current start to grow at the same moment as in Figure 14, but the rate of growth is at first very slow, so it takes some time before the increase becomes visible. The current extreme values, which occur approximately at the bad weather boundaries $x = 0.45$ and $x = 0.55$, are not attained until $s = 1$. This is the point of time, when the current sources are turned off. The voltage along the line then has maxima in the same positions as the current extreme values and a minimum at $x = 0.5$. When the sources are turned off, a discharge of the capacitors is started. Discharge currents, directed from the voltage peak positions to the right and to the left, develop. The presence of memory in the capacitors implies that some time must elapse before the discharge currents are fully developed. Hence, the line current, observed at $s = 1$, only breaks down slowly. The magnetic field, lingering in the inductors, also tends to preserve the current. The shape of the current wave at $s > 1$ can be understood in the following way: when the current sources are turned off, this can qualitatively be comprehended as current sources of the same size, but with opposite directions being switched on at $s = 1$, thus canceling the original ones. The new current sources give rise to a current wave in the opposite direction from the wave excited at $s = 0$. The total current can be obtained by superposition.

The Figures 16–17 show the current $i(x, s)$ and the voltage $v(x, s)$, respectively, for a calculation with $G_0 = 1.5 \cdot 10^{-5}$ and $\chi_0 = 0.7 \cdot 10^{-5}$. Observe that in order to visualize all details, the angle of view has been chosen differently in Figure 17, than in Figures 16. With less memory, the process is more rapid, than in Figure 15, so i and v grow quicker. Detailed studies indicate a small decrease in current prior to the moment when the current sources are turned off at $s = 1$. This is due to discharge of the capacitors through the shunt conductance G. With less memory and the access to easy discharge through the growing shunt conductance G, the decrease in i for $s > 1$ is more rapid than in Figure 15. For the voltage curve, the discharge through G is even quicker. A voltage peak is immediately built up over the capacitors of the source area and then as rapidly torn down by discharge through G. A similar voltage behaviour can be seen outside the very source area; more pronounced in the vicinity of the sources. One detail hidden in Figure 17 should be pointed out: immediately after $s = 1$, a negative voltage peak develops around $x = 0.5$, and then quickly discharges through the shunt conductance G. A qualitative explanation can

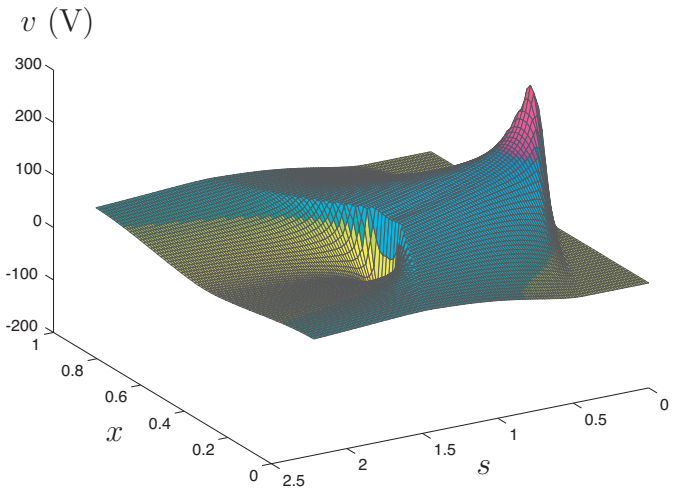

Figure 17: Voltage waves from current sources—$G_0 = 1.5{\cdot}10^{-5}$ and $\chi_0 = 0.7{\cdot}10^{-5}$.

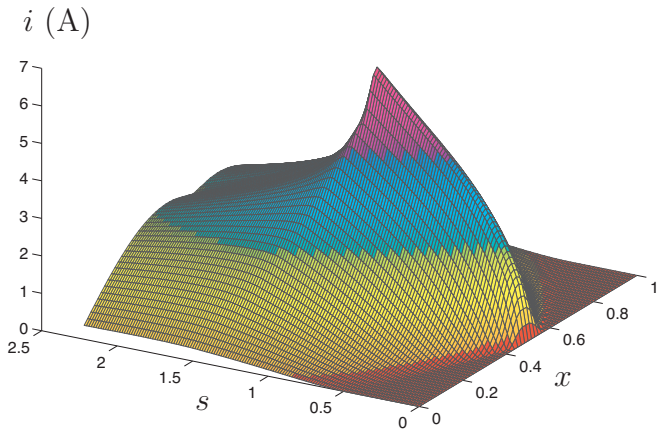

Figure 18: Current waves from voltage sources—$G_0 = 1.5{\cdot}10^{-5}$ and $\chi_0 = 0.7{\cdot}10^{-5}$.

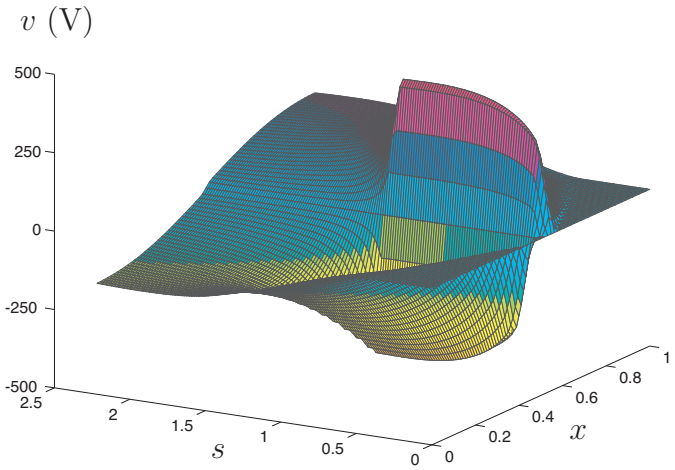

Figure 19: Voltage waves from voltage sources—$G_0 = 1.5{\cdot}10^{-5}$ and $\chi_0 = 0.7{\cdot}10^{-5}$.

be found by a superposition of voltage waves from current sources with opposite directions.

Finally, the Figures 18–19 show the current and voltage waves on a transmission line supplied from internal voltage sources in the middle part. The choice of parameters is $G_0 = 1.5 \cdot 10^{-5}$ and $\chi_0 = 0.7 \cdot 10^{-5}$. The number of mesh-intervals is 128×288. Observe that with voltage sources, the response is reversed: the current i is even, and the voltage v is odd as a function of x around $x = 0.5$. From the symmetry in v, it follows that there are discharge currents through the shunt conductance G with opposite directions. This reduces the effect, so the main discharge current follows the transmission line. In a calculation similar to Figure 14, but with voltage sources, it can be seen that since there is no net discharge through G, the current stays constant until the voltage sources are turned off. The actual shapes of the graphs in the Figures 18–19 can be explained by a discussion similar to the one above.

5 Conclusions

The new time domain method offers a way to calculate direct waves from internal sources in non-stationary media numerically. The comparison with an alternative, partially analytical solution of the Klein-Gordon equation shows that the results from the two calculations conform. A by-product in the derivation of the alternative method is a new identity of the Bessel function J_1. Waves on the transmission line, initiated by square pulses from current or voltage sources, demonstrate complex variations, depending on the size of the shunt capacitance dispersion. If the susceptibility kernel χ_e is increased, the waves require longer time intervals to develop, and after the source is disconnected, the discharge is slowed down. In the case of current sources, a short cut is provided by the exponentially growing shunt conductance of the source area. This helps to speed up the attenuation of the waves. With voltage sources, there are discharge currents in opposite directions. Therefore, the net influence of the shunt conductance on the attenuation is insignificant.

Acknowledgment

The work reported in this paper is supported by a grant from the Swedish Research Council for Engineering Sciences and their support is gratefully acknowledged.

References

[1] I. Åberg and A. Karlsson. "The source problem"—transient waves propagating from internal sources in non-stationary media". *Wave Motion*, 1997. (in press).

[2] I. Åberg, G. Kristensson, and D.J.N. Wall. Propagation of transient electromagnetic waves in time-varying media—direct and inverse scattering problems. *Inverse Problems*, **11**(1), 29–49, 1995.

[3] I. Åberg, G. Kristensson, and D.J.N. Wall. Transient waves in non-stationary media. *J. Math. Phys.*, **37**(5), 2229–2252, 1996.

[4] V.A. Ambarzumian. Diffuse Reflection of Light by a Foggy Medium. *Compt. Rend. Acad. Sci. SSR.*, **38**, 229, 1943.

[5] R.S. Beezley and R.J. Krueger. An electromagnetic inverse problem for dispersive media. *J. Math. Phys.*, **26**(2), 317–325, 1985.

[6] H. Bremmer. The W.K.B. approximation as the first term of a geometrical-optical series. *Comm. Pure Appl. Math.*, **4**, 105–115, 1951.

[7] S. Chandrasekhar. *Radiative Transfer*. Dover, New York, 1960.

[8] J.P. Corones. Bremmer series that correct parabolic approximations. *J. Math. Anal. Appl.*, **50**, 361–372, 1975.

[9] J.P. Corones, M.E. Davison, and R.J. Krueger. Direct and inverse scattering in the time domain via invariant imbedding equations. *J. Acoust. Soc. Am.*, **74**(5), 1535–1541, 1983.

[10] J.P. Corones and R.J. Krueger. Obtaining scattering kernels using invariant imbedding. *J. Math. Anal. Appl.*, **95**, 393–415, 1983.

[11] J.P. Corones and Z. Sun. Simultaneous reconstruction of material and transient source parameters using the invariant imbedding method. *J. Math. Phys.*, **34**(5), 1824–1845, 1993.

[12] R. Courant and D. Hilbert. *Methods of Mathematical Physics*, volume 2. Interscience, New York, 1962.

[13] M.E. Davison and R.C. Winther. A general approach to splitting and invariant imbedding for linear wave equations. *J. Math. Anal. Appl.*, **188**(1), 158–181, 1994.

[14] J. Fridén. Inverse scattering for the homogeneous dispersive anisotropic slab using transient electromagnetic fields. *Wave Motion*, **23**(4), 289–306, 1996.

[15] K.L. Kreider. Time dependent direct and inverse electromagnetic scattering for the dispersive cylinder. *Wave Motion*, **11**, 427–440, 1989.

[16] G. Kristensson. Transient electromagnetic wave propagation in waveguides. *J. Electro. Waves Applic.*, **9**(5/6), 645–671, 1995.

[17] G. Kristensson and R.J. Krueger. Direct and inverse scattering in the time domain for a dissipative wave equation. Part 1: Scattering operators. *J. Math. Phys.*, **27**(6), 1667–1682, 1986.

[18] G. Kristensson and S. Rikte. Scattering of transient electromagnetic waves in reciprocal bi-isotropic media. *J. Electro. Waves Applic.*, **6**(11), 1517–1535, 1992.

[19] R.J. Krueger and R.L. Ochs, Jr. A Green's function approach to the determination of internal fields. *Wave Motion*, **11**, 525–543, 1989.

[20] J. Lundstedt. Condition for distortionfree transmission lines with a nonuniform characteristic impedance. *IEEE Trans. Microwave Theory Tech.*, **43**(6), 1386–1389, 1995.

[21] M. Norgren and S. He. Reconstruction of the constitutive parameters for an Ω material in a rectangular waveguide. *IEEE Trans. Microwave Theory Tech.*, **43**(6), 1315–1321, 1995.

[22] H. Otterheim. *Time domain direct and inverse scattering for gyrotropic media*. PhD thesis, Royal institute of technology, Stockholm, Sweden, 1993.

[23] F.G. Tricomi. *Integral Equations*. Dover, New York, 1957.

[24] H.S. Tzou. *Piezoelectric Shells*. Kluwer, Dordrecht, 1993.

[25] V.H. Weston. Invariant imbedding and wave splitting in $\mathbb{R}^3$: II. The Green function approach to inverse scattering. *Inverse Problems*, **8**, 919–947, 1992.

[26] W.H. Weston and S. He. Wave splitting of the telegraph equation in $\mathbb{R}^3$ and its application to inverse scattering. *Inverse Problems*, **9**(6), 789–812, 1993.

[27] E. Zauderer. *Partial Differential Equations of Applied Mathematics*. Wiley, New York, second edition, 1989.